Plasma Phys. Control. Fusion **50** (2008) 025009 (15pp) doi:10.1088/0741-3335/50/2/025009

Magnetized plasma–wall transition—consequences for wall sputtering and erosion

S Devaux[1] **and G Manfredi**[2]

[1] Laboratoire de Physique des Milieux Ionisés et Applications, CNRS and Université Henri Poincaré, F-54506 Vandoeuvre-les-Nancy, France
[2] Institut de Physique et Chimie des Matériaux de Strasbourg, CNRS and Université Louis Pasteur BP 43, F-67034 Strasbourg, France

E-mail: Stephane.Devaux@lpmi.uhp-nancy.fr and Giovanni.Manfredi@ipcms.u-strasbg.fr

Received 25 October 2007, in final form 11 December 2007
Published 10 January 2008
Online at stacks.iop.org/PPCF/50/025009

Abstract
The ion distribution function in front of an absorbing wall is computed using a kinetic model. The ions' energy and angle of impact are of particular importance, as they determine the level of wall erosion and sputtering. Their dependence on the plasma parameters (magnitude and angle of incidence of the magnetic field, ion and electron temperatures, etc) is investigated in detail. We conclude that a magnetic field with grazing incidence and a low electron-to-ion temperature ratio have a beneficial effect, as far as wall erosion and sputtering are concerned.

(Some figures in this article are in colour only in the electronic version)

1. Introduction

Although the study of the transition between a plasma and a wall is as old as plasma physics itself, it is still a very active research field, especially in relation to the physics of nuclear fusion devices [1]. Plasma–wall interactions play a crucial role in a wide range of laboratory and even geophysical plasmas (bombardment of a satellite by charged particles). For instance, in order to interpret correctly the measurements obtained with a Langmuir probe or a retarding-field analyzer (RFA), it is necessary to understand how the probe surface disturbs the plasma surrounding it [2].

In fusion devices, the study of plasma–wall interactions is of paramount importance, because the surfaces in contact with the plasma (limiters, divertors, antennas, etc) are eroded by ion and neutral bombardment and may thus see their lifetime considerably reduced [3, 4]. The erosion also releases high-Z impurities, which migrate towards the bulk plasma and, due to radiation, deteriorate its confinement [1]. In order to keep within reasonable limits the erosion of different wall materials, it is important to estimate the plasma characteristics in the region in contact with the wall. Of particular importance are the particles and energy fluxes, and the ion energy and angular distribution on the wall.

Because of the presence of the surface itself, the ion distribution in front of the wall is generally not Maxwellian. Indeed, even for an unmagnetized plasma, the presence of sheaths can substantially deform the ion distribution, as was observed in numerical simulations and laboratory experiments [5–8]. For magnetized plasmas, the distribution can even feature several peaks at different energies, which further complicates the estimation of the wall erosion [9].

The transition between a perfectly absorbing wall and an unmagnetized plasma at thermodynamical equilibrium is composed of two regions. The Debye sheath (DS) is a thin, positively charged region located just in front of the wall and tends to shield the negative electric charge of the wall. The DS is stable if the ions enter the sheath at a speed larger than the ion sound speed, a condition known as the 'Bohm criterion' [10]. As the ions velocity is generally smaller in the bulk plasma, this condition requires the existence of an intermediate region where the ions are accelerated towards the wall. This acceleration occurs in the collisional presheath (CP), which is a quasineutral region dominated by ion–neutral collisions. The DS extends over a region of a few Debye lengths λ_{De}, and is therefore much thinner than the CP, whose typical scale is given by the ion–neutral mean free path λ_{mfp}.

When a tilted magnetic field is applied, a new quasineutral region—the magnetic presheath (MP)—appears between the CP and the DS. The thickness of the magnetic presheath is governed by the ion Larmor radius ρ_{i}, and for fusion devices and laboratory plasmas [11] the following ordering is generally satisfied: $\lambda_{\mathrm{De}} \ll \rho_{\mathrm{i}} \ll \lambda_{\mathrm{mfp}}$ [12].

Along their travel from the plasma to the wall, the ions are first accelerated along the magnetic fields lines in the CP; then they are progressively reoriented towards the wall in the MP; and finally, in the DS, they are strongly accelerated in the direction normal to the wall [9, 13]. We will show that, during this process, the ion distribution is significantly distorted and can be very far from a Maxwellian on the wall. This can lead to the existence of several ion populations, displaying different energy and angular distributions. Each of these populations is therefore associated with a different sputtering rate [14, 15].

In this paper, we use a kinetic Vlasov code to compute the ion distribution at the wall, in the presence of a magnetic field and weak ion–neutral collisions. The code has been described and validated in previous works [9, 16], where it was used to study the plasma–wall transition region in detail. Here, we concentrate on the ion distribution on the wall and its impact on the sputtering and erosion of the material surface. In particular, we investigate the influence of the intensity and the angle of incidence of the external magnetic field.

2. Model

2.1. Kinetic plasma model

Our work aims to simulate the interaction between a steady-state plasma and a perfectly absorbing wall. A homogeneous magnetic field $\boldsymbol{B}$ lies in the xOy plane and makes an angle α with the Oy direction, as shown in figure 1. The wall is located at $x = 0$ and the bulk plasma occupies the region $x \geqslant x_{\mathrm{p}}$. As the wall is supposed to be infinite in the yOz plane, the physical system is invariant by translation in this plane: the study can thus be reduced to one dimension in space and three dimensions in velocity, yielding a '1D3V' problem.

The adopted model is based on the evolution of the ion distribution function in phase space $f(x, \boldsymbol{v}, t)$, which is governed by a modified Vlasov equation,

$$\frac{\partial f_{\mathrm{i}}}{\partial t} + v_x \frac{\partial f_{\mathrm{i}}}{\partial x} + \frac{e}{m_{\mathrm{i}}}(\boldsymbol{E} + \boldsymbol{v} \times \boldsymbol{B}) \cdot \frac{\partial f_{\mathrm{i}}}{\partial \boldsymbol{v}} = -\nu(f_{\mathrm{i}} - f_0), \tag{1}$$

where $\boldsymbol{E}$ and $\boldsymbol{B}$ are the electric and magnetic fields, e is the elementary electric charge and m_{i}

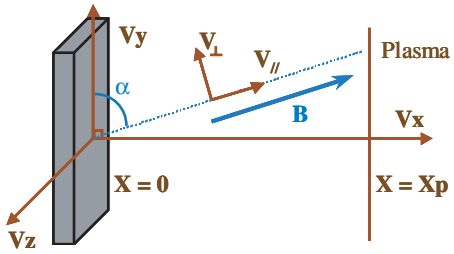

Figure 1. Geometry of the problem. The wall is located at $x = 0$ and the equilibrium plasma at $x > x_p$. The magnetic field $\boldsymbol{B}$ field lies in the xOy plane and makes an angle α with the Oy direction.

is the ion mass; x is the position coordinate normal to the wall and $\boldsymbol{v}$ the velocity vector. The term added on the right-hand side of equation (1) is a generalized Bathnagar–Gross–Krook (BGK) collisonal term, which models the effects of ionization and ion–neutral collisions. This BGK term tends to rebuild the equilibrium Maxwellian distribution $f_0(\boldsymbol{v})$—characterized by a temperature T_{i0} and a density n_{i0}—in a typical time given by ν^{-1}, where $\nu = v_{thi}/\lambda_{mfp}$ is the collision frequency, v_{thi} being the ion thermal speed in the plasma and λ_{mfp} the ion–neutral mean free path. $f_0(v)$ also represents the ion distribution in the bulk plasma, where the ions are assumed to be at thermodynamic equilibrium with the neutrals, and therefore it is used as a boundary condition for f_i at $x = x_p$.

Whereas the magnetic field is assumed to be purely external, the electric field is self-consistent, i.e. it is created by the charged particles in the plasma and obeys Poisson's equation:

$$\frac{\partial^2 \phi}{\partial x^2} = -\frac{e}{\epsilon_0}(n_i - n_e), \tag{2}$$

where ϵ_0 is the vacuum dielectric constant; the ion density n_i is directly computed from the ion distribution function: $n_i = \int f_i \mathrm{d}\boldsymbol{v}$. The electrons are assumed to be at thermodynamic equilibrium with temperature T_e, so that their density is obtained from the Boltzmann relation:

$$n_e(\phi) = n_0 \exp\left(\frac{e\phi}{k_B T_e}\right), \tag{3}$$

where n_0 is the density in the bulk plasma and k_B is the Boltzmann constant; ϕ is the electric potential related to electric field via $E_x = -\partial\phi/\partial x$.

The electric potential is set to zero on the plasma side ($x = x_p$), whereas at the wall ($x = 0$) a floating potential condition is assumed, given by the accumulation of electric charges on the wall. The floating potential is computed by integrating Ampère's equation on the wall:

$$\frac{\partial E_x}{\partial t} = -\frac{e}{\epsilon_0}(J_i - J_e). \tag{4}$$

The ion flux towards the wall is given by $J_i = \int v_x f_i \mathrm{d}\boldsymbol{v}$. The electron flux is estimated by assuming a half-Maxwellian velocity distribution for the electrons, which yields

$$J_e(0, t) = n_0 \left(\frac{k_B T_e}{2\pi m_e}\right)^{1/2} \exp\left(\frac{e\phi(0)}{k_B T_e}\right). \tag{5}$$

We also assumed that, under the physical conditions considered in our simulations, secondary electron emission at the wall is negligible. We are aware that one should be cautious with this hypothesis, as a small amount of secondary electrons can affect the structure of the plasma–wall transition [17].

In order to obtain the steady-state solution of equation (1), we perform a time-dependent calculation using a Vlasov Eulerian code [9, 18, 19]. Each run begins with a spatially homogeneous plasma at thermodynamic equilibrium (ion Maxwellian distribution at temperature T_{i0}) in the whole transition region between $x = 0$ and $x = x_p$. The plasma is let to evolve according to the Vlasov–Poisson system until it reaches a (inhomogeneous) steady state. The run is stopped when the spatial profiles of physically relevant quantities (e.g. density, average velocity) do not evolve significantly anymore [16].

2.2. Wall erosion model

A complete description of the physical sputtering caused by the ions impinging on a wall needs to take into account a wide range of parameters. Such a description should include, among others, a model for the interaction between the impinging particle and the first atomic layers of the surface, the binding energy, the temperature of the material, etc [20, 21]. In this work, we are mainly concerned with the dependence of the total sputtering yield Y on some crucial plasma parameters, particularly the magnitude of the external magnetic field B and its angle of incidence α. Therefore, we will neglect all atomic-physics issues that depend on the ion species and on the type of target. Typically, our results will provide the sputtering yield $Y(B, \alpha)$, normalized to the value it takes for normal incidence $Y_0(\alpha = 90^\circ)$, which does not depend on B.

For a single impinging ion, the sputtering yield is mainly a function of two parameters that are independent of the type of material or the ion species: the angle θ under which the ion strikes the wall and its kinetic energy E_{kin}. This reflects the fact that removing an atom from a surface is easier when the ion strikes the surface at grazing incidence. Indeed, for normal incidence, the atom is mainly 'pushed' further inside the surface, whereas for grazing incidence it can be more easily ejected.

Several empirical formulae have been proposed in the past to fit the experimental measurements of the sputtering yield. The Bohdanski formula [21] (for normal ion incidence) expresses the sputtering yield as a function of the energy of the impinging ions, as well as a number of other parameters characterizing the projectile and target atoms. Yamamura [21, 22] proposed a formula for the angular dependence of the sputtering yield. Both formulae contain several fitting parameters that need to be adjusted to the experimental data.

Here, our purpose is mainly to provide a rough estimate of the sputtering yield for an ion population that has travelled through the presheath and sheath regions, and is therefore considerably distorted compared with a Maxwellian distribution. In order to do so, we make the simplifying assumption that the sputtering yield is directly proportional to the ion energy and inversely proportional to the sine of the impact angle (note that our convention for the impact angle differs from that adopted in most other works on sputtering). Thus, the sputtering yield peaks for $\theta = 0^\circ$, even though experimental evidence suggests that the maximum should be attained for $90^\circ \gg \theta_{opt} > 0^\circ$. However, in the cases of interest here, most ions strike the surface with angles larger than 30°, so that the existence of a peak at small angles should not be relevant.

Under these assumptions, the sputtering yield Y associated with a single impinging ion can be written as $Y \propto E_{kin}/\sin\theta$. In a plasma, an entire population of ions (which is in general not Maxwellian) comes into contact with the surface [23]. The sputtering yield must then be computed using the ion velocity distribution on the wall. The kinetic energy is readily obtained from the relation: $E_{kin} = \frac{1}{2}m_i(v_x^2 + v_y^2 + v_z^2)$, whereas θ is given by the following expression

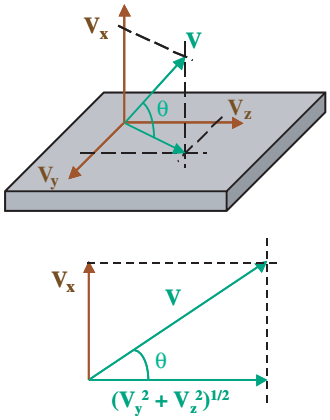

Figure 2. The angle of incidence θ is the angle between the velocity vector $\vec{v}$ and its projection on the (v_y, v_z) plane (where the wall lies). The bottom part of the figure represents the plane defined by v_x and $\vec{v}$. Note that this representation is slightly different from that of figure1.

(see figure 2):

$$\theta = \arctan\left(\frac{v_x}{\sqrt{v_y^2 + v_z^2}}\right). \tag{6}$$

Using $E_{\rm kin}$ and θ, we are able to estimate the sputtering yield for different values of the magnitude and the intensity of the external magnetic field.

3. Numerical results

3.1. Ion distribution on the wall

In a previous study [9], we have shown that varying the intensity and the incidence of $\boldsymbol{B}$ leads to significantly different ion distributions on the wall. In order to assess this point more precisely, we provide a set of figures (figure 3) where we plot the ion velocity distribution on the wall, in the (v_x, v_y) plane (i.e. the plane that contains the magnetic field). On each plot, the distribution function is represented by isodensity contour lines. Negative velocities are velocities directed towards the wall; the dashed line and the dashed–dotted line represent, respectively, the directions parallel and perpendicular to $\boldsymbol{B}$ in the xOy plane. The intensity of the magnetic field is measured by the dimensionless quantity $\omega = \omega_{\rm ci}/\omega_{\rm pi}$, the ratio of the ion cyclotron frequency to the ion plasma frequency. Reading figure 3 from left to right, the intensity of the magnetic field decreases from $\omega = 0.1$ to $\omega = 0.01$; while reading the figure from top to bottom, the angle of incidence increases from $\alpha = 10^\circ$ to $\alpha = 40^\circ$. The other relevant parameters of the simulations are the temperature ratio $\tau = T_{\rm e}/T_{\rm i} = 10$ and the normalized collision frequency $\nu/\omega_{\rm pi} = 10^{-3}$.

The top left plot in figure 3 ($\omega = 0.10$ and $\alpha = 10^\circ$) corresponds to a case where the influence of the magnetic field is clearly visible. The distribution is characterized by a dominant body centered at $v_x = -7.85 v_{\rm thi}$ and $v_y = -5.0 v_{\rm thi}$ and a thin tail of particles extending in the v_y direction up to $v_y = 0$. The main population is due to ions that have been accelerated along the magnetic field lines in the CP, then reoriented towards the wall in the MP, and finally strongly accelerated in the DS: this population has thus gained a large velocity in both the v_x

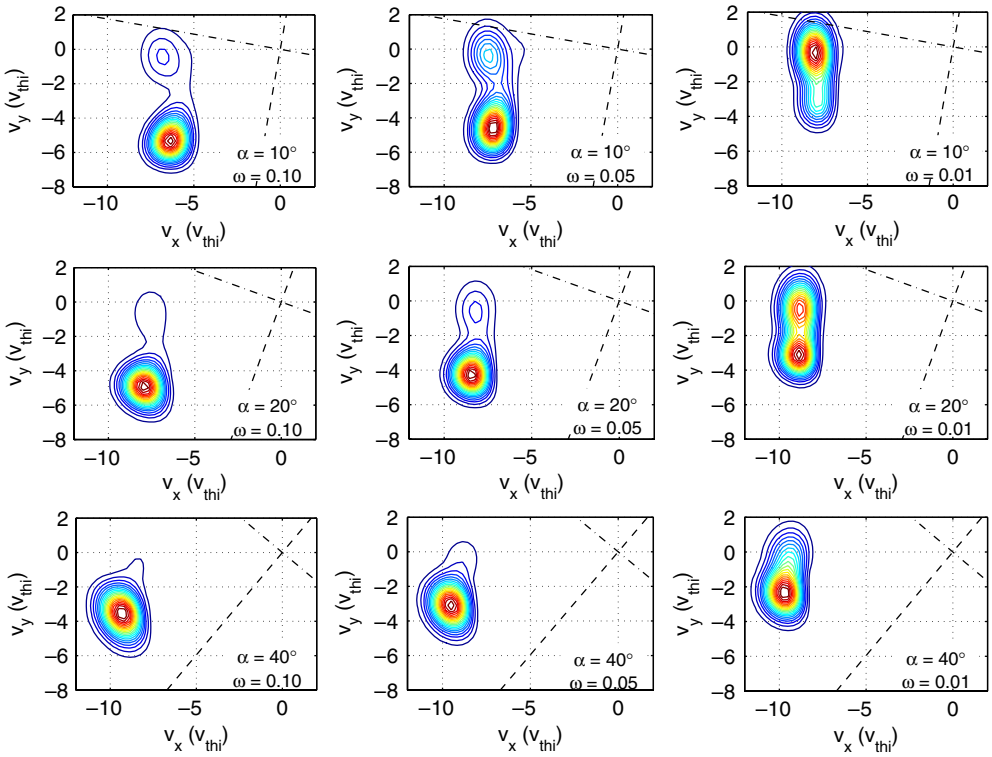

Figure 3. Ion distribution function on the wall in the (v_x, v_y) plane, for various values of the incidence of the magnetic field α and its normalized magnitude ω. ω decreases from 0.1 to 0.01 (left to right) and α increases from 10° to 40° (top to bottom). The dashed and dashed–dotted lines represent, respectively, the directions parallel and perpendicular to the magnetic field. All simulations were performed with $\tau = 10$ and $\nu/\omega_{\mathrm{pi}} = 10^{-3}$.

and the v_y directions. Particles found in the tail are those that underwent a collision with a neutral atom too close to the wall to be again accelerated along the magnetic field lines. These ions have roughly the same velocity distribution along the v_x direction as the main population, but a lower velocity in the v_y direction.

When the intensity ω is decreased, the magnetic field is not strong enough to force the ions to travel along its field lines. As a consequence, the number of particles located in the tail increases with decreasing ω, and the tail becomes more populated than the main body for $\omega = 0.01$ and $\alpha = 10°$.

Increasing the angle of incidence α has the opposite effect and the tail progressively disappears, while the main body of the distribution moves to slightly smaller velocities in v_y. This is easily understood by noting that, for larger angles of incidence, the direction parallel to $\boldsymbol{B}$ becomes closer to the direction normal to the wall. Therefore, the acceleration along the magnetic field lines in the CP results in a moderate increase in the v_y velocity. Effectively, the main body and the tail merge in a single-hump distribution, such as that visible in the bottom left plot of figure 3 ($\omega = 0.1$ and $\alpha = 40°$).

As these two populations (main body and tail) are associated with rather different kinetic energies and angles of incidence on the surface, we can anticipate that both the intensity and the incidence of the magnetic field will have an influence on the sputtering yield.

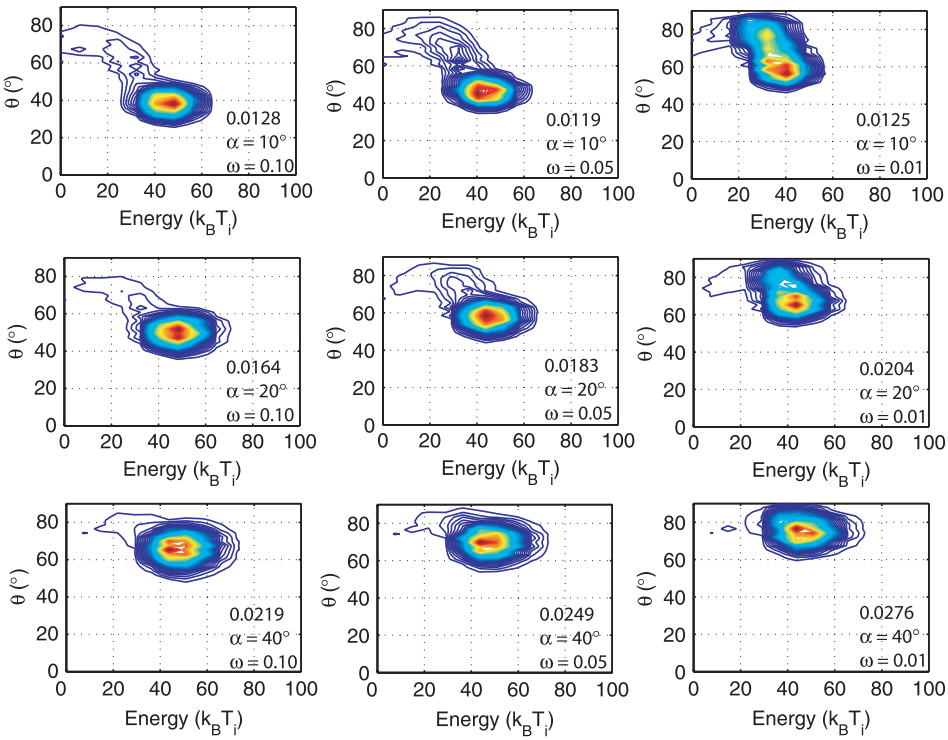

Figure 4. Ion distribution function on the wall in the energy–angle plane, for various values of the incidence of the magnetic field α and its normalized magnitude ω. ω decreases from 0.1 to 0.01 (left to right) and α increases from 10° to 40° (top to bottom). The number given at the bottom right corner of each plot is the value of the maximum of the distribution function, in arbitrary units. All simulations were performed with $\tau = 10$ and $\nu/\omega_{\rm pi} = 10^{-3}$.

We now study the ion distribution on the wall as a function of the kinetic energy and the angle of incidence of the ions, which is defined so as to satisfy the relation: $F(E_{\rm kin}, \theta){\rm d}E_{\rm kin}{\rm d}\theta = f(\boldsymbol{v}){\rm d}\boldsymbol{v}$. $F(E_{\rm kin}, \theta)$ is plotted in figure 4 for several values of ω and α, following the same structure used in figure 3.

The energy–angle distribution basically reproduces the effects observed in the (v_x, v_y) distribution. For instance, for $\alpha = 10^\circ$ and $\omega = 0.05$, the main body of the distribution is centered at $E_{\rm kin} = 45 k_{\rm B} T_{\rm i}$ and $\theta = 50^\circ$ and a tail appears at lower energies and larger angles. This is consistent with the fact that the tail corresponds to an ion population with $v_y \simeq 0$ and same v_x as the main body of the distribution: this results in a lower kinetic energy and an angle of incidence closer to $\theta \simeq 0^\circ$, because the distribution tail has an almost normal incidence. We also notice that, for the main body of the distribution, the energy peak is almost independent of α and ω. Indeed, for these ions, the gain in energy is mainly determined by the acceleration parallel to $\boldsymbol{B}$ in the CP and by the subsequent acceleration along x in the DS. Such effects do not depend on the intensity and the inclination of the magnetic field, and therefore lead to an energy increase that is largely independent of these two quantities.

The number given at the bottom right corner of each plot is the value of the maximum of the distribution function, in arbitrary units. When α decreases, the decrease in the angle of impact θ for ions located in the main body of the distribution is accompanied by a decrease in the number of ions present in it. This means that the main body of the distribution is depleted with respect to the tail, which may have important consequences on the sputtering yield.

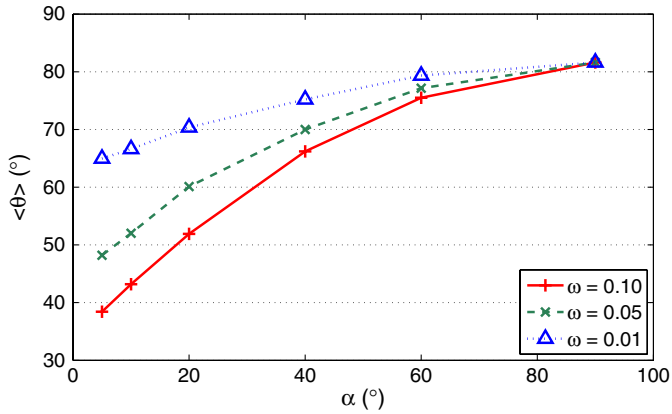

Figure 5. Average angle of impact on the wall as a function of the incidence of the magnetic field α and its magnitude ω. $\omega = 0.01$ (triangles); $\omega = 0.05$ (stars); $\omega = 0.1$ (crosses).

3.2. Sputtering-relevant quantities

In order to understand the influence of the computed ion distributions on the wall erosion, we need to extract some appropriate averaged quantities. Here, we will concentrate on the energy of the impinging particles, their angle of incidence, and their density on the wall. We will illustrate the dependence of these quantities on the intensity and inclination of the external magnetic field.

We present, in figure 5, the behavior of the average angle of incidence $\langle\theta\rangle$ of the ions striking the wall (see equation (6)). As expected, $\langle\theta\rangle$ is larger than α: this is because the large electric field present in the DS is very efficient in reorienting the ions along the direction normal to the wall. This effect is more important when α is small, and for $\alpha \to 90^\circ$ the incidence is almost normal and independent of the magnetic field intensity. The consequence is a lower sputtering yield than what could be naively expected by assuming that the ions are constantly accelerated along the magnetic field lines.

The average kinetic energy $\langle E_{\rm kin}\rangle$ is depicted in figure 6. It decreases rapidly with decreasing α, whereas it is less sensitive to the intensity of the magnetic field (it decreases slightly with ω). A grazing incidence of the magnetic field is therefore favorable to reduce the sputtering yield. The behavior of the *average* kinetic energy is to be contrasted with the energy of the peak of the main body of the ion distribution. Whereas the former decreases with α, the latter is roughly constant, as we had deduced from figure 4. The decrease in $\langle E_{\rm kin}\rangle$ is thus due to the appearance of a low-energy tail in the ion distribution.

In figure 7 we plot the maximum value of f attained in the main body of the distribution function (peak at $v_y < 0$ in figure 3), normalized to the total number of ions on the wall. This quantity slightly increases for incidence angles larger than 40°, but drops rapidly for $\alpha \leqslant 20^\circ$—the drop is more pronounced for the cases where the magnetic field is weak. For $\omega = 0.01$ and $\alpha = 10^\circ$ and 5°, the 'main body' of the distribution is so depleted that no clear peak is visible anymore (this is the reason why these points are not represented in figure 7).

This behavior (already visible in figure 3 for $\omega = 0.01$) can be readily explained by noting that a lower ω corresponds to a relatively greater importance of collisions, which tend to favor normal incidence for the impinging ions. This is an important result as far as sputtering is concerned, because it shows that, by decreasing α and ω, the ions gradually leave the main body of the distribution (associated with grazing impact angles, and thus high sputtering yields) and

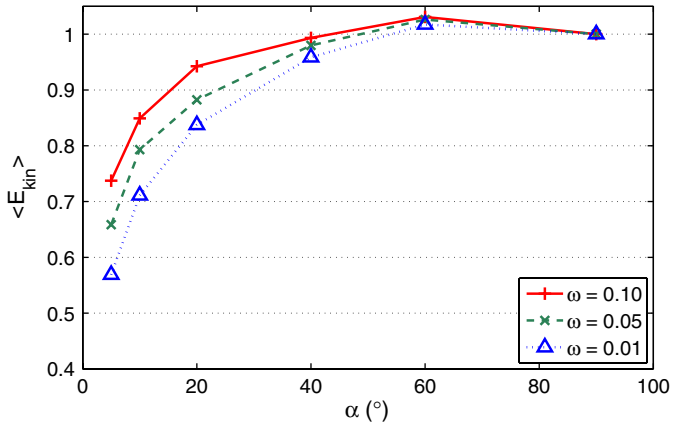

Figure 6. Average kinetic energy of the ions impinging on the wall as a function of the incidence of the magnetic field α and its magnitude ω. The energy is normalized to its value for $\alpha = 90°$. $\omega = 0.01$ (triangles); $\omega = 0.05$ (stars); $\omega = 0.1$ (crosses).

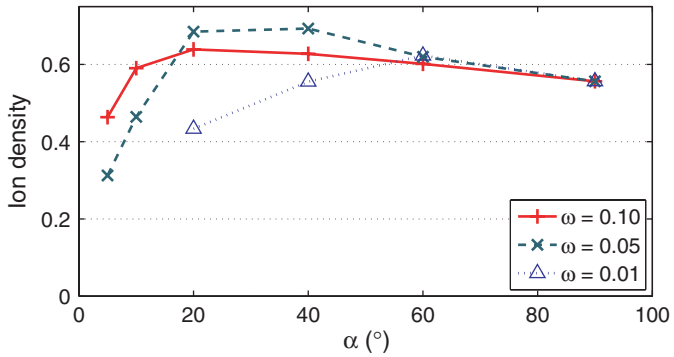

Figure 7. Peak of the main body of the ion velocity distribution (normalized to the total number of ions on the wall), as a function of the incidence of the magnetic field α and its magnitude ω.

populate the distribution tail (associated with normal impact angles and low sputtering yields). This effect is also at the origin of the relatively weak dependence of the average angle of impact $\langle\theta\rangle$ with the angle of incidence of the magnetic field (figure 5).

Finally, we show an estimate of the total sputtering yield (normalized to the value computed for normal incidence) due to the ion distribution on the wall (figure 8):

$$Y(\alpha, \omega) \propto \int_0^{\infty} \int_0^{\pi/2} \frac{E_{\rm kin}}{\sin\theta} F(\theta, E_{\rm kin}) \mathrm{d}\theta \, \mathrm{d}E_{\rm kin}. \tag{7}$$

Clearly, the sputtering yield decreases significantly with α, an effect that may seem surprising, as a grazier angle of impact should correspond to a larger sputtering yield. In fact, the sputtering yield depends on the number of impinging ions, as well as on their energy and angle of impact. Due to the presence of the DS, the angle of impact is relatively large, even for low α, while the energy drops rapidly with α, the net effect being a decrease in the sputtering yield. In tokamaks, the angle of incidence of the magnetic field on the wall (divertor) is of the order of a few degrees: this aims at spreading the ion flux on a larger surface, thus reducing the heat flow on the wall. The present results show that a grazing incidence is also beneficial as far as wall erosion is concerned.

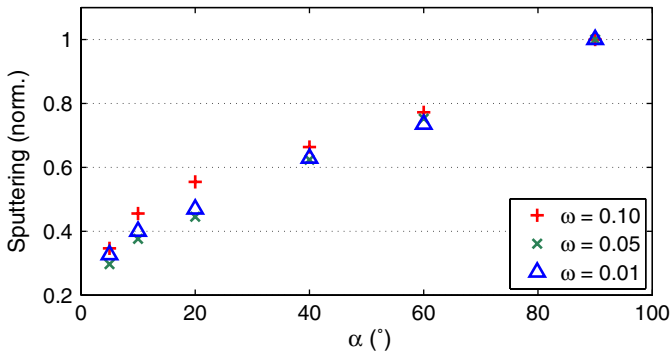

Figure 8. Sputtering yield (normalized to its value for $\alpha = 90°$), as a function of the incidence of the magnetic field α and its magnitude ω.

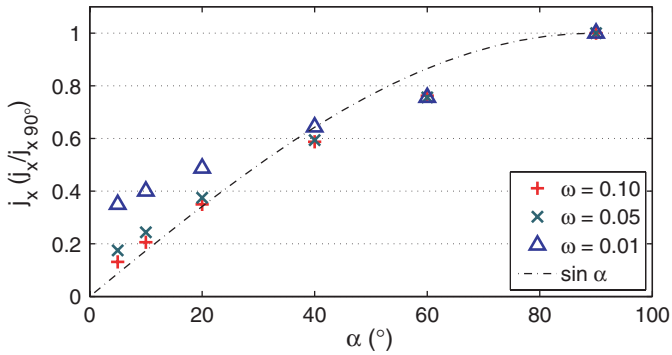

Figure 9. Particles flux (normalized to its value for $\alpha = 90°$), as a function of the incidence of the magnetic field α and its magnitude ω.

3.3. Heat and particles fluxes

The particles and heat fluxes on the wall are defined, respectively, as follows:

$$J_x = \int v_x f(\boldsymbol{v})\, \mathrm{d}\boldsymbol{v}, \tag{8}$$

$$Q_x = \int v_x E_{\mathrm{kin}} f(\boldsymbol{v})\, \mathrm{d}\boldsymbol{v}. \tag{9}$$

They are plotted in figures 9 and 10 and, as expected, both decrease with α. Interestingly, for large values of the magnetic field ($\omega \geqslant 0.05$) the fluxes become independent of ω and converge to the simple formula Q_x, $J_x \propto \sin\alpha$, which is what should be expected if the ions were simply accelerated along the magnetic field lines. For the particle flux, this can be explained by noting that the ions are purely accelerated along $\boldsymbol{B}$ in the CP, so that at the magnetic presheath entrance (MPE), J_x obeys a '$\sin\alpha$' law. The particles flux is then (almost) conserved in the MP and the DS, so that the dependence of J_x on the wall just reflects the acceleration occurring in the CP.

For the heat flux, things are slightly more complex. At the MPE, Q_x will also obey a '$\sin\alpha$' law. Further, it can be proven that, in the absence of collisions (i.e. mainly in the MP and

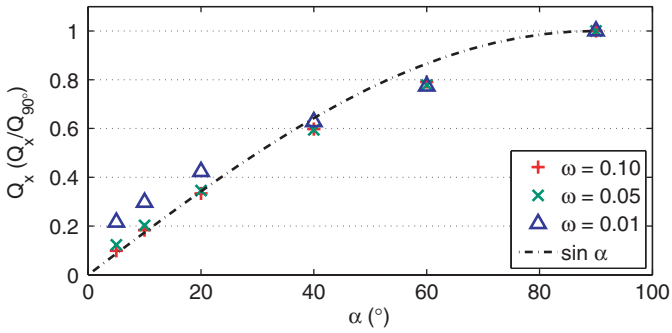

Figure 10. Heat flux (normalized to its value for $\alpha = 90^\circ$), as a function of the incidence of the magnetic field α and its magnitude ω.

DS), the following quantity is conserved along the plasma–wall transition: $R_x \equiv Q_x + e\phi J_x$. We can therefore write

$$Q_x^{\text{wall}} = Q_x^{\text{MPE}} + J_x^{\text{MPE}} e\Delta\phi, \tag{10}$$

where $\Delta\phi$ represents the potential drop between the MPE and the wall, and we have used the fact that J_x is conserved between the MPE and the wall. It is well known that $\Delta\phi$ is almost independent of α [13]: for $\alpha \simeq 90^\circ$ the drop takes place almost entirely in the DS, whereas for $\alpha \ll 90^\circ$ it occurs mainly in the MP, but the total drop is virtually the same. As all other quantities in equation (10) behave as $\sin\alpha$, we deduce for the heat flux on the wall: $Q_x \propto \sin\alpha$.

For smaller values of the magnetic field, the relative effect of collisions (measured by the normalized collision rate, here $\nu/\omega_{\text{pi}} = 10^{-3}$) increases with respect to magnetic effects. The size of the MP scales as ω^{-1} [9, 24] and, for a sufficiently small ω, it will approach the size of the CP. Then, collisions can no longer be neglected in the MP and the argument put forward in the previous paragraph breaks down. For vanishing magnetic field, the fluxes obviously become independent of α.

3.4. Temperature dependence

In this section, we investigate the influence of the temperature ratio, $\tau = T_{\text{e}}/T_{\text{i}}$, on the sputtering-relevant quantities analysed above. In the previous sections, the temperature ratio was fixed at $\tau = 10$, which is appropriate for low-pressure plasma discharges, but not for tokamak edge plasmas, where τ is of order unity (in the scrape-off layer, the ions are even slightly hotter than the electrons).

Figures 11 and 12 show the average kinetic energy and angle of impact of the ions as a function of the temperature ratio. Whereas the angle is virtually insensitive to τ, the kinetic energy decreases roughly linearly with τ, which is consistent with the well-known fact that the total potential drop across the sheath and presheaths is proportional to T_{e}. As a result, the sputtering yield (figure 13) and the heat flux on the wall (figure 14) also decrease with the temperature ratio.

Finally, looking at the ion velocity distribution on the wall (figure 15), we see that the double-humped distribution observed for $\tau = 10$ is no longer present for $\tau = 1$. This is because, for smaller temperature ratios, the ions are less strongly accelerated in the presheath region. These accelerated ions then acquire a smaller velocity in the v_y direction and their distribution merges with that of the ions having undergone many collisions, which peaks around $v_y = 0$.

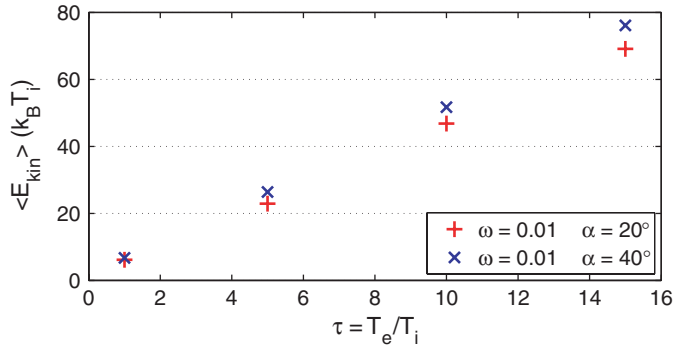

Figure 11. Average kinetic energy of the ions impinging on the wall (normalized to the bulk ion temperature) as a function of the temperature ratio, for $\omega = 0.01$ and $\alpha = 20^\circ$ and 40°.

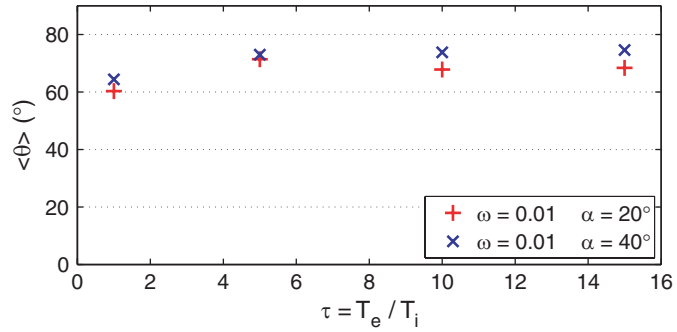

Figure 12. Average impact angle of the ions on the wall as a function of the temperature ratio, for $\omega = 0.01$ and $\alpha = 20^\circ$ and 40°.

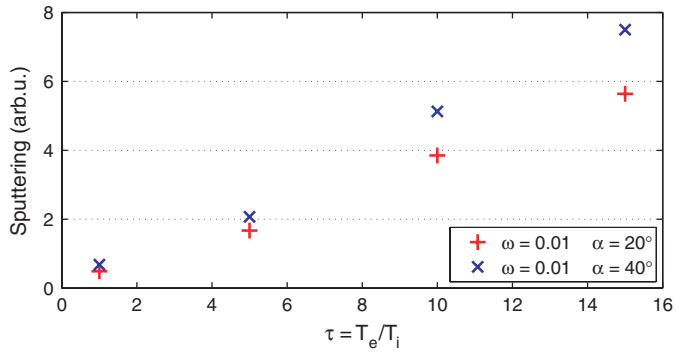

Figure 13. Sputtering yield as a function of the temperature ratio, in arbitrary units, for $\omega = 0.01$ and $\alpha = 20^\circ$ and 40°.

In spite of the absence of the two peaks, the sputtering rate for $\tau = 1$ nevertheless decreases with the angle of incidence of the magnetic field, as shown in figure 16. Thus, most conclusions drawn in the previous sections still seem to hold for temperature ratios closer to those observed in tokamak plasmas.

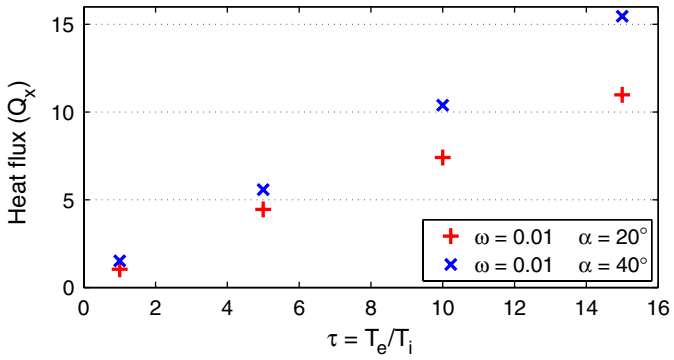

Figure 14. Heat flux on the wall as a function of the temperature ratio, in arbitrary units, for $\omega = 0.01$ and $\alpha = 20^\circ$ and 40°.

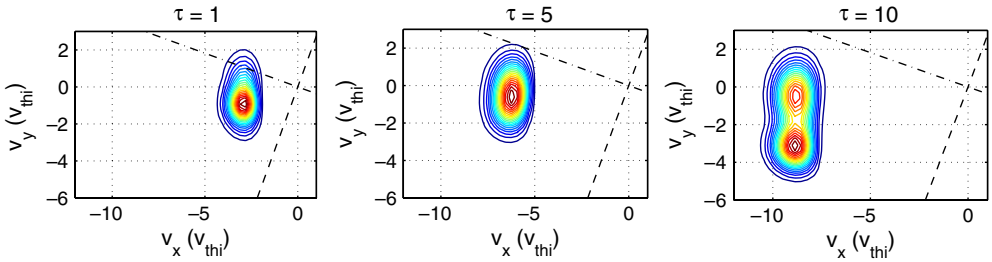

Figure 15. Ion distribution function on the wall in the (v_x, v_y) plane, for $\alpha = 20^\circ$, $\omega = 0.01$, and three values of the temperature ratio $\tau = 1$, 5 and 10 (from left to right).

4. Conclusion

A material surface immersed in an ionized gas is exposed to constant bombardment by energetic particles. In the long run, this bombardment will erode the outer layers of the surface and shorten, sometimes considerably, its useful lifetime. In a plasma, the impinging particles (ions) display a broad distribution in both kinetic energy and angle of impact, which are the two main parameters determining the level of sputtering and erosion. It is therefore important to know the ion phase space distribution on the surface in order to estimate its lifetime.

In this work, we have made use of a kinetic Vlasov code to determine the ion velocity distribution on the wall. Due to the presence of the presheaths and Debye sheath, the ion distribution is significantly deformed with respect to the equilibrium Maxwellian. Interestingly, we observed that two different ion populations can be present at the wall, giving rise to a two-peak velocity distribution. These two populations correspond respectively to ions that have been drifting without collisions along the magnetic field lines and to ions that have experienced several collisions before hitting the wall.

The simulations showed that, even for relatively strong magnetic fields, the average angle of incidence of the impinging ions is never as grazing as the angle α between the magnetic field and the wall. This is because, in the DS, the electric field manages to partially redirect the ions along the direction normal to the surface. The average kinetic energy also decreases with α, the net effect being a smaller sputtering yield for grazing magnetic field incidence. As the particles and heat fluxes also drop with α (due to a simple geometric effect), our study

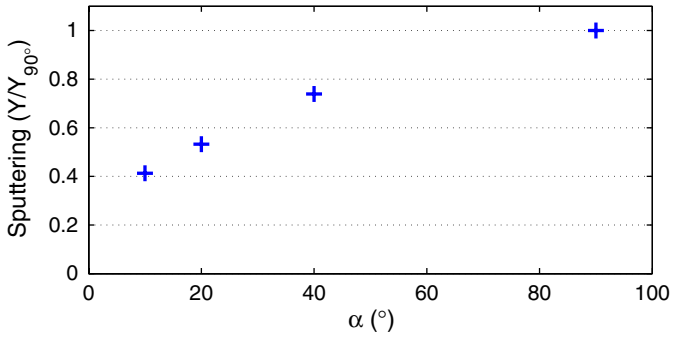

Figure 16. Sputtering yield as a function of the angle α (normalized to its value for $\alpha = 90^\circ$), for $\tau = 1$ and $\omega = 0.01$.

confirms that a grazing incidence has the beneficial effect of reducing the impact of energetic ion bombardment on the wall.

The previous results were obtained for a temperature ratio $\tau = 10$, relevant to low-pressure laboratory plasma experiments. For tokamak edge plasmas, the temperature ratio is closer to unity. Numerical experiments confirmed that the above behavior is still observed for $\tau = 1$ and showed that the sputtering yield and heat flux on the wall decrease with the temperature ratio.

All simulations have been restricted to angles of incidence larger than $\alpha = 5^\circ$. Although this is reasonable for tokamak edge plasmas, the relevant value for ITER would be slightly smaller, around $\alpha = 2^\circ$. The model adopted here, however, is limited by the fact that we assume highly magnetized electrons, which follow the magnetic field lines with no cross-field transport. For small angles, this assumption is no longer valid, as can be shown by the following simple calculation. On the wall, the electron flux due to convective transport in the direction parallel to $\boldsymbol{B}$ can be written as $J_e^{\parallel} \simeq n_e v_{the} \sin\alpha$, where v_{the} is the electron thermal velocity and n_e the electron density (see equation (5)). The electronic collisional transport in the direction perpendicular to $\boldsymbol{B}$ (which, for small angles, almost coincides with the normal to the wall), can be represented by a suitable Fick's law: $J_e^{coll} = -D_\perp \nabla_\perp n_e$, with diffusion coefficient $D_\perp = \rho_e^2 \omega_{ce}$, where ρ_e is the electron Larmor radius and ω_{ce} the electron cyclotron frequency. By equating the convective and collisional fluxes, we obtain a critical angle, $\alpha_c = \rho_e / L_\perp$, below which collisional electron transport cannot be neglected. Here, $L_\perp \equiv |n_e / \nabla_\perp n_e|$ is the typical variation of the electron density in the DS, which is approximately $L_\perp \approx 5\lambda_{De}$. Using dimensionless variables, the critical angle finally takes the form

$$\alpha_c \simeq 0.2 \times \sqrt{\frac{m_e}{m_i}} \frac{\omega_{pi}}{\omega_{ci}}. \tag{11}$$

For a deuterium plasma with $n_e = 10^{18}$ m^{-3} and $B = 4$ T (which is relevant for ITER edge plasmas), we obtain $\omega_{pi}/\omega_{ci} \approx 5$, which yields a critical angle $\alpha_c \approx 1^\circ$. A more refined model for the electron dynamics would thus be necessary to investigate the regime of extremely grazing incidence. However, all our results show a clear trend towards lower sputtering for decreasing angles of incidence and it is unlikely that this trend be reversed for very small values of α.

Finally, we point out that a quantitatively sound determination of wall sputtering and erosion would require a precise knowledge of the target surface and of the atomic physics parameters related to it, which we did not take into account in our study. However, our simulated distribution functions could be used as input data for numerical codes that compute

the sputtering yield, which often assume a Maxwellian distribution for simplicity [23]. Using more realistic ion distributions, such as those provided here, should improve the accuracy of the sputtering estimation.

References

[1] Stangeby P C 2000 *The Plasma Boundary of Magnetic Fusion Devices* (London: Institute of Physics Publishing)
[2] Valsaque F, Manfredi G, Gunn J P and Gauthier E 2002 *Phys. Plasmas* **9** 1806
[3] Janeschitz G 2001 ITER JCT and HTs 2001 *J. Nucl. Mater.* **290–293** 1
[4] Behrisch R, Federici G, Kukushkin A and Reiter D 2003 *J. Nucl. Mater.* **313–316** 388
[5] Chung K-S and Hutchinson I H 1988 *Phys. Rev.* A **38** 4721
[6] Riemann K-U 1991 *J. Appl. Phys.* D **24** 493
[7] Tskhakaya D, Eliasson B, Shukla P K and Kuhn S 2004 *Phys. Plasmas* **11** 3945
[8] Riemann K-U 2000 *J. Tech. Phys.* **41** 89
[9] Devaux S and Manfredi G 2006 *Phys. Plasmas* **13** 083504
[10] Bohm D 1949 *The Characteristics of Electrical Discharges in Magnetic Fields* ed A Guthrie and R K Wakerling (New York: McGraw-Hill)
[11] Gravier E, Brochard F, Bonhomme G, Pierre T and Briançon J-L 2004 *Phys. Plasmas* **11** 529
[12] Ahedo E 1997 *Phys. Plasmas* **4** 4419
[13] Chodura R 1982 *Phys. Fluids* **25** 1628
[14] Seeböck R J 1999 *Surf. Coat. Technol.* **166–119** 564
[15] Parks P B and Lippmann S I 1994 *Phys. Plasmas* **1** 3883
[16] Manfredi G and Valsaque F 2004 *Comput. Phys. Commun.* **164** 262
[17] Tskhakaya D, Kuhn S, Petrzilka V and Khanal R 2002 *Phys. Plasmas* **9** 2486
[18] Cheng C Z and Knorr G 1976 *J. Comput. Phys.* **22** 330
[19] Fijalkow E 1999 *Comput. Phys. Commun.* **116** 319
[20] Eckstein W 1997 *J. Nucl. Mater.* **248** 1
[21] Garcia-Rosales C, Eckstein W and Roth J 1995 *J. Nucl. Mater.* **218** 8
[22] Eckstein W 2005 *Nucl. Instrum. Methods Phys. Res.* **232** 108
[23] Roth J, Eckstein W and Guseva M 1997 *Fusion Eng. Des.* **37** 465
[24] Chodura R 1986 *Physics of Plasma–Wall Interactions in Controlled Fusion* ed D E Post and R Behrisch (New York: Plenum) p 99